Numerical Calculation of Eigensolutions of 3D Shapes Using the Method of Fundamental Solutions

Pedro R. S. Antunes
Group of Mathematical Physics of the University of Lisbon, Complexo Interdisciplinar, Av. Prof. Gama Pinto 2, P-1649-003 Lisboa, Portugal

Received 2 September 2009; accepted 5 February 2010
Published online in Wiley InterScience (www.interscience.wiley.com).
DOI 10.1002/num.20594

In this work, we study the application of the Method of Fundamental Solutions (MFS) for the calculation of eigenfrequencies and eigenmodes in two and three-dimensional domains. We address some mathematical results about properties of the single layer operator related to the eigenfrequencies. Moreover, we propose algorithms for the distribution of the collocation and source points of the MFS in three-dimensional domains which is an extension of the choices considered by Alves and Antunes (CMC 2(2005), 251–266) for the two-dimensional case. Also the application of the Plane Waves Method is investigated. Several examples with Dirichlet and Neumann boundary conditions are considered to illustrate the performance of the proposed methods. Numer Methods Partial Differential Eq 000: 000–000, 2010

Keywords: meshfree methods; method of fundamental solutions; room acoustics; acoustic resonance

I. INTRODUCTION

Let $\Omega \subset \mathbb{R}^d$ (with $d = 2$ or $d = 3$) be a bounded domain with regular boundary $\Gamma = \partial\Omega$. We will consider the Dirichlet eigenvalue problem for the Laplace operator. This is equivalent to finding the frequencies κ such that there exists $u \not\equiv 0$ which satisfies the Dirichlet boundary value problem for the Helmholtz equation,

$$\begin{cases} \Delta u + \kappa^2 u = 0 & \text{in } \Omega, \\ u = 0 & \text{on } \Gamma. \end{cases} \tag{1}$$

Another possibility is to consider the Neumann problem, where the boundary condition in problem (1) is replaced by $\partial_n u = 0$ on Γ. As an application in acoustics, this corresponds to calculating the resonance frequencies κ associated with a drum (in the two dimensional case) or the eigenfrequencies of a cavity or a room (in the three-dimensional case).

Correspondence to: Pedro R. S. Antunes, Group of Mathematical Physics of the University of Lisbon, Complexo Interdisciplinar, Av. Prof. Gama Pinto 2, P-1649-003 Lisboa, Portugal (e-mail: pant@cii.fc.ul.pt)

There are a few domains with simple geometries such as balls or rectangular domains for which we have an explicit formula for the eigensolutions. For more general shapes the solution of the eigenvalue problem (1) requires the use of a numerical method for PDEs. The finite difference method and the finite element method have been widely used. However these methods require extra computational effort associated to the generation of a mesh which is a difficult task especially for a three-dimensional problem. Another possibility is to apply the boundary element method (e.g., [1]) but this requires dealing with the integration of weakly singular kernels on the boundary. Recently, another class of methods, known as meshless methods have received much attention (e.g., [2–6]). These methods avoid the construction of a mesh and avoid integration calculations which makes their application to complicated geometries very simple. A disadvantage is that the system matrices are ill conditioned.

In this work, we study the application of a meshless method, the method of fundamental solutions (MFS) which has been applied since the 1960s (e.g., [7–9]). The MFS falls in a general class of approaches called Trefftz methods. This type of methods consists in the solution of a boundary value problem by a linear combination of some trial functions that satisfy the PDE of the problem. In this context, it is important to have sets of solutions for which completeness and convergence can be guaranteed (cf. [10, 11]). The MFS is a Trefttz method where the particular solutions are obtained translating the fundamental solution of the PDE to some source points outside the domain. The coefficients are then calculated such that the approximation fits the boundary conditions of the problem in some sense. This method is applicable to any elliptic boundary value problem, provided the fundamental solution of the PDE is known.

The application of the MFS to the solution of the eigenvalue problem (1) was introduced by Karageorghis in [12] and applied for simple 2D shapes. The multiply connected case with simple geometries was addressed in [13] and [14] and it was found that the method yields spurious eigenfrequencies. The analytical studies for annular domains revealed that those eigenfrequencies are related with the interior artificial boundary. However, this analysis is not general and is applicable only for a small class of annular domains with concentric balls. We will provide some mathematical justification for a more general case.

It is well known that the location of the source points is very important to obtain accurate approximations for a general shaped domain. In [15], a particular choice was proposed which leads to very accurate results in the calculation of eigensolutions of two-dimensional domains. Here we propose the extension of this choice to the three-dimensional case. Moreover, we address the application of the Method of Plane Waves for the eigenvalue problem.

II. PROPERTIES OF THE SINGLE LAYER OPERATOR RELATED TO THE EIGENFREQUENCIES

The MFS is a well-known numerical method for solving partial differential equations. The idea is to approximate the solution by a linear combination of point sources $\Phi_\omega(\cdot - y)$ given by a fundamental solution of the PDE. The singularities must lie at the exterior of the domain. For the Helmholtz equation usually we take

$$\Phi_\omega(x) = \frac{i}{4} H_0^{(1)}(\omega|x|) \tag{2}$$

for the two-dimensional case, where $|.|$ denotes the euclidean norm in $\mathbb{R}^d$ and $H_0^{(1)}$ is the first Hänkel function and

$$\Phi_\omega(x) = \frac{e^{i\omega|x|}}{4\pi\,|x|} \tag{3}$$

for the three-dimensional case. The MFS can be related to the discretization of the single layer potential

$$(\mathbf{L}_\omega\varphi)(x) = \int_{\hat{\Gamma}} \Phi(x-y)\varphi(y)ds_y \approx u_N(x) = \sum_{j=1}^{N} \alpha_{N,j}\Phi_\omega(x-y_{N,j}),\ x \notin \hat{\Gamma} \tag{4}$$

where $\hat{\Gamma}$ is the boundary of a domain $\hat{\Omega}$ such that $\hat{\Omega} \supset \bar{\Omega}$ (eg. [16]). The source points $y_{N,j}$ are taken on $\hat{\Gamma}$. We next prove some properties of the operator $\mathbf{L}_\omega$ related to the eigenfrequencies which allow to justify the numerical algorithms for the eigensolutions that will be used. The restriction of $\mathbf{L}_\omega$ to Ω will be denoted by $\mathcal{T}_\Omega\mathbf{L}_\omega$, the trace of $\mathbf{L}_\omega$ to $\partial\Omega$ will be denoted by $\mathcal{T}^0_{\partial\Omega}\mathbf{L}_\omega$ and the trace of the normal derivative to $\partial\Omega$ will be denoted by $\mathcal{T}^1_{\partial\Omega}\mathbf{L}_\omega$.

Theorem 1. *Suppose that Ω is a bounded simply connected domain with regular boundary. Then,*

(i) If $\omega \in \mathbb{R}$, then $Ker(\mathcal{T}_\Omega\mathbf{L}_\omega) = \{0\}$.
(ii) If ω is not an eigenfrequency of the interior Dirichlet problem in Ω then $dim(Ker(\mathcal{T}^0_{\partial\Omega}\mathbf{L}_\omega)) = 0$.
(iii) If for a certain frequency ω we have $dim(Ker(\mathcal{T}^0_{\partial\Omega}\mathbf{L}_\omega)) = m \in \mathbb{N}$, then ω is an eigenfrequency of the interior Dirichlet problem and it has multiplicity at least m.

Proof.

(i) By the analiticity of $\mathbf{L}_\omega\varphi$, $\mathbf{L}_\omega\varphi = 0$ in Ω implies $\mathbf{L}_\omega\varphi = 0$ in $\hat{\Omega}$ and the continuity of the traces implies $(\mathbf{L}_\omega\varphi)^+ = (\mathbf{L}_\omega\varphi)^- = 0$ on $\hat{\Gamma}$. Since $\omega \in \mathbb{R}$, then ω cannot be a scattering pole for the exterior problem. By the well posedness of the exterior Dirichlet problem, with the Sommerfeld radiation condition (verified by $\mathbf{L}_\omega\varphi$), this implies $\mathbf{L}_\omega\varphi = 0$ and $\varphi = 0$ because φ is the jump of the normal derivative of $\mathbf{L}_\omega\varphi$ at the boundary.

(ii) If ω is not a Dirichlet eigenfrequency of Ω then $\mathcal{T}^0_{\partial\Omega}\mathbf{L}_\omega\varphi = 0$ implies that $\mathcal{T}_\Omega\mathbf{L}_\omega\varphi = 0$ and by (i) we have $\dim(Ker(\mathcal{T}^0_{\partial\Omega}\mathbf{L}_\omega)) = 0$.

(iii) We first prove that if for a certain frequency ω there exists a density $\varphi \in Ker(\mathcal{T}^0_{\partial\Omega}\mathbf{L}_\omega)\backslash\{0\}$, then $\mathcal{T}_\Omega\mathbf{L}_\omega\varphi$ is an eigenfunction of the interior Dirichlet problem associated to the eigenfrequency ω, which is the counterpart of (ii). We only need to prove that $\mathcal{T}_\Omega\mathbf{L}_\omega\varphi$ is not identically zero. Suppose that $\mathcal{T}_\Omega\mathbf{L}_\omega\varphi \equiv 0$, then by (i) we have $\varphi = 0$ and we get a contradiction. Now if $\dim(Ker(\mathcal{T}^0_{\partial\Omega}\mathbf{L}_\omega)) = m$, then we have m non trivial densities $\varphi_1, \ldots, \varphi_m$ which are linearly independent on $\hat{\Gamma}$ and therefore each function $\mathcal{T}_\Omega\mathbf{L}_\omega\varphi_i$, $i = 1, \ldots, m$ is an eigenfunction. Now we will prove that they are linearly independent eigenfunctions, which implies that the multiplicity of the eigenfrequency is at least equal to m. Suppose that $\sum_{i=1}^m \alpha_i\ \mathcal{T}_\Omega\mathbf{L}_\omega(\varphi_i) \equiv 0$, then by linearity we have $\mathcal{T}_\Omega\mathbf{L}_\omega(\sum_{i=1}^m \alpha_i\varphi_i) \equiv 0$. Now, by (i) we have $\sum_{i=1}^m \alpha_i\ \varphi_i = 0$ on $\hat{\Gamma}$ which implies that $\alpha_1 = \cdots = \alpha_m = 0$ (since the densities are linearly independent) and then $\mathcal{T}_\Omega\mathbf{L}_\omega\varphi_i$, $i = 1, \ldots, m$ are linearly independent eigenfunctions. ∎

Remark 1. For the Neumann case, if ω is not an eigenfrequency of Ω, then $\mathcal{T}^1_{\partial\Omega}\mathbf{L}_\omega\varphi(x) = 0$ implies $\mathcal{T}_\Omega\mathbf{L}_\omega\varphi = 0$ and this implies $\varphi = 0$.

Thus, using Theorem 1 (ii), the procedure to find the Dirichlet eigenfrequencies that we will adopt is to search for ω such that $\dim(Ker(\mathcal{T}^0_{\partial\Omega}\mathbf{L}_\omega)) \neq 0$ and to calculate the eigenfrequencies for the Neumann problem, as the frequencies for which we have non trivial solutions that satisfy $\mathcal{T}^1_{\partial\Omega}\mathbf{L}_\omega\varphi(x) = 0, x \in \partial\Omega$.

Instead of using the single layer potencial approach, the double layer potential representation for $x \notin \hat{\Gamma}$ may be used,

$$\mathbf{D}_\omega\psi(x) = \int_{\hat{\Gamma}} \partial_{n_y}\Phi_\omega(x-y)\psi(y)\,ds_y \approx u_N(x) = \sum_{j=1}^{N} \beta_{N,j}\partial_n\Phi_\omega(x-y_{N,j}) \tag{5}$$

where ∂_n denotes the outward normal derivative at the point $y_{N,j}$. For this case, results similar to Theorem 1 using the continuity of the traces of the normal derivative of $\mathbf{D}_\omega$ on the boundary $\hat{\Gamma}$ can be obtained. The normal trace of the double layer potential is hypersingular, and it can be defined using Hadamard finite parts.

In [13] and [14], the application of the MFS to multiply connected domains was studied and the appearance of spurious eigenfrequencies was found. However, the analytic study that was developed using degenerate kernels is only applicable to some annular domains with concentric balls. We are able to give some mathematical justification for a more general case. In order to maintain simplicity we assume that the domain has only one hole but all the considerations are easily extended to the case of several holes. Consider the problem in Ω which is bounded by two surfaces Γ_1 and Γ_2,

$$\begin{cases} \Delta u + \kappa^2 u = 0 & \text{in } \Omega, \\ B_1(x) = 0 & \text{on } \Gamma_1, \\ B_2(x) = 0 & \text{on } \Gamma_2, \end{cases} \tag{6}$$

with $\partial\Omega = \Gamma_1 \cup \Gamma_2$, for a non zero function u. The boundary conditions B_1 and B_2 can be of Dirichlet or Neumann type. The source set is composed by two surfaces $\hat{\Gamma}_1$ and $\hat{\Gamma}_2$ which are chosen to be the boundaries of domains $\hat{\Omega}_1$ and $\hat{\Omega}_2$, such that Γ_2 surrounds $\hat{\Omega}_2$ and $\hat{\Gamma}_1$ surrounds

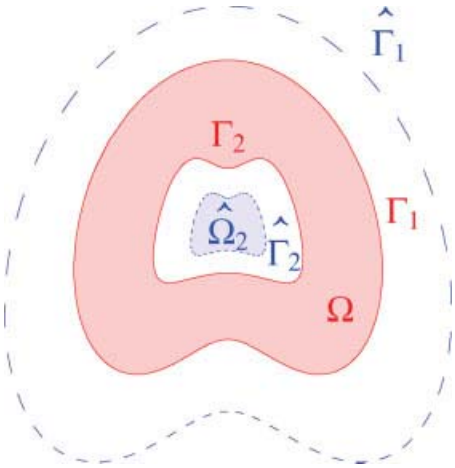

FIG. 1. The boundaries for a domain with a hole. [Color figure can be viewed in the online issue, which is available at www.interscience.wiley.com.]

the domain Ω as showed in Figure 1. In that case we define $\hat{\Gamma} = \hat{\Gamma}_1 \cup \hat{\Gamma}_2$. The next result shows that if we adopt the single layer potential in the MFS formulation, then in the multiply connected problem we have as spurious solutions, the eigenfrequencies of a Dirichlet interior eigenvalue problem with boundary $\hat{\Gamma}_2$. We will denote by $\Lambda(D)$ the set of Dirichlet eigenfrequencies of the domain D.

Theorem 2. *If $\omega \in \Lambda(\hat{\Omega}_2)$ and $\mathcal{T}_{\hat{\Omega}_2}\mathbf{L}_\omega$ is not identically null, then $dim(Ker(\mathcal{T}^0_{\partial\Omega}\mathbf{L}_\omega)) > 0$.*

Proof. Let $\varphi \in Ker(\mathcal{T}^0_{\partial\Omega}\mathbf{L}_\omega)\backslash\{0\}$, then $\mathbf{L}_\omega\varphi$ vanishes on Γ_1 and Γ_2. If $\mathcal{T}_\Omega\mathbf{L}_\omega\varphi$ is not identically null, then automatically $\dim(Ker(\mathcal{T}^0_{\partial\Omega}\mathbf{L}_\omega)) > 0$ and the Theorem is proved. If $\mathcal{T}_\Omega\mathbf{L}_\omega\varphi$ is identically null, then by analytic extension and continuity of the trace on $\hat{\Gamma}_1$ we have homogeneous exterior problem. Now $\omega \in \Lambda(\hat{\Omega}_2)$ which implies that $\omega \in \mathbb{R}$. Then by the well posedness of the exterior problem (the Sommerfeld radiation condition is also satisfied) we have $\mathbf{L}_\omega\varphi = 0$ in $\mathbb{R}^d\backslash\hat{\Omega}_2$. Now by the continuity of the traces on $\hat{\Gamma}_2$ we have an interior homogeneous eigenvalue problem, and by the hypothesis that $\mathcal{T}_{\hat{\Omega}_2}\mathbf{L}_\omega\varphi$ is not identically null, the conclusion follows. ∎

III. NUMERICAL ALGORITHM FOR THE STANDARD MFS

In this section, we will describe the numerical algorithm for the calculation of eigensolutions using the MFS. We consider mainly regular domains. For an extension to domains with corners or cracks see [17].

To define the matrix of the MFS system we must choose the collocation points and the source points. In the case of the circle and the square, Karageorghis obtained very good results placing the source points on a curve which was an expansion of the boundary $\partial\Omega$ (cf. [12]). However, for a more general shape we must consider an appropriate choice (cf. [15]).

A. Algorithm for the Choice of the Collocation and Source Points—3D

We will consider a particular distribution of the collocation points and point sources which is an extension of the choice proposed in [15] for the two-dimensional case.

Choice of the Collocation Points—3D. We consider the boundary of a domain Ω which can be parametrized by

$$\Gamma = \left\{ f(t,s) : \ (t,s) \in [0,2\pi[\times \left[-\frac{\pi}{2}, \frac{\pi}{2} \right] \right\}$$

and choose an integer number p, the number of planes. Given $t^* \in [0,2\pi[$ we define the curve

$$\Gamma_0 = \left\{ f(t^*,s) : \ s \in \left[-\frac{\pi}{2}, \frac{\pi}{2} \right] \right\}$$

and calculate the values s_i, with $s_0 = -\frac{\pi}{2} < s_1 < s_2 < \cdots < s_p = \frac{\pi}{2}$ such that we have

$$|f(t^*,s_i) - f(t^*,s_{i+1})| = \frac{|\Gamma_0|}{p} := \zeta.$$

Then, on each of the curves

$$\gamma_i = \{ f(t,s_i) : \ t \in [0,2\pi[\}$$

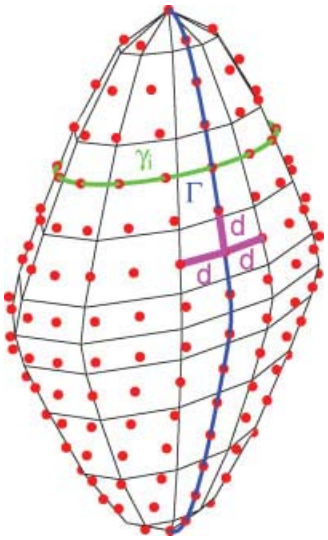

FIG. 2. Distribution of the collocation points. [Color figure can be viewed in the online issue, which is available at www.interscience.wiley.com.]

we place $\left\lceil \frac{|\gamma_i|}{\zeta} \right\rceil$ points uniformly distributed if $|\gamma_i| > 0$. If $|\gamma_i| = 0$ we consider just the collocation point $f(t^*, s_i)$ (Fig. 2).

Choice of the Source Points—3D. The source points are calculated in the following way: for each collocation point x_i we calculate $y_i = x_i + \alpha \frac{\tilde{n}}{\|\tilde{n}\|}$, where $\tilde{n}$ is an approximation of the vector which is normal to the boundary $\partial\Omega$ at the point x_i. When the boundary of the domain is given by a parametrization $f(t, s)$ this can be exactly calculated by

$$\tilde{n} = \pm \partial_t f(t, s) \times \partial_s f(t, s),$$

choosing the sign such that the vector points to the exterior of the domain at each collocation point x_i. In Figure 3, we illustrate the choice of the source points.

As for the 2D case, the parameter α is a constant and its magnitude depends on the geometry of the domain and on the dimension of the system such that the quantity $N\alpha/|\Omega|$ can not be too large. Usually for simple geometries the convergence is faster for a larger value of α. However, when we increase the number of source points, the condition number also increase. Thus, for more complicated shapes for which we must consider a larger number of source points to have satisfactory approximations, we must choose a smaller value of α to have not too big condition number. A simple way to calculate the optimal value of α is to use an algorithm similar to the one that was studied in [18].

B. Numerical Calculation of the Eigenfrequencies

Using Theorem 1 we search for the frequencies ω for which $\dim(Ker(\mathcal{T}^0_{\partial\Omega}\mathcal{S}_\omega)) \neq 0$. Defining N collocation points $x_i \in \partial\Omega$ and N source points $y_{N,j} \in \hat{\Gamma}$, we obtain the system

$$\sum_{j=1}^{N} \alpha_{N,j} \Phi_\omega(x_i - y_{N,j}) = 0, \quad (x_i \in \partial\Omega). \tag{7}$$

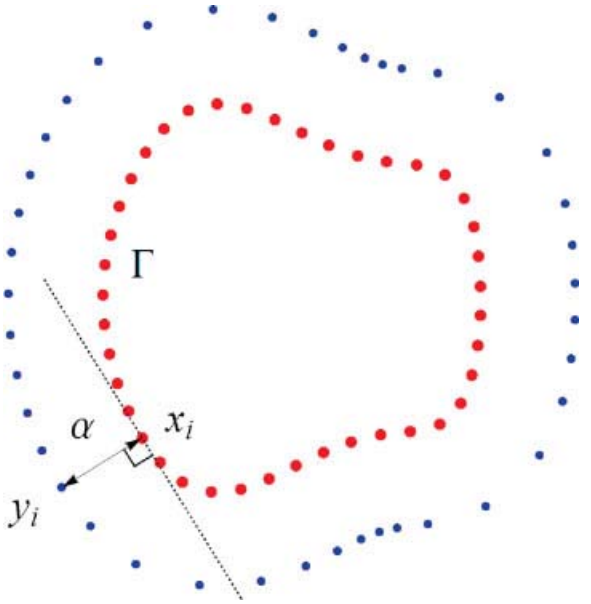

FIG. 3. Choice of the source points. [Color figure can be viewed in the online issue, which is available at www.interscience.wiley.com.]

The numerical approximations for the eigenfrequencies are the values ω such that the MFS matrix

$$\mathbf{A}(\omega) = [\Phi_\omega(x_i - y_j)]_{N\times N} \tag{8}$$

has a null determinant or equivalently, such that the function $g(w) := \log|Det[\mathbf{A}(w)]|$ has a singularity. To calculate them we use a descent method—the golden ratio search (see [15] for details).

Remark 2. The determinant of the matrix is a complex number, but the eigenfrequencies are real numbers. Then it is expected that the imaginary parts of the frequencies for which the matrix is not invertible are not very significant when compared to their real parts. We preferred to look for the absolute value of the determinant of the matrix. Another possibility is the strategy adopted by Karageorghis in [12] who calculated the zeros of the real and imaginary parts separately.

C. Numerical Calculation of the Eigenmodes

To obtain the eigenmodes we start calculating an approximate eigenfrequency $\tilde{\kappa}$. The approximation of the eigenmode is given by

$$\tilde{u}(x) = \sum_{j=1}^{N+1} \alpha_j \Phi_{\tilde{\kappa}}(x - y_j). \tag{9}$$

To avoid the trivial solution $\tilde{u}(x) \equiv 0$, we use a collocation method on $N+1$ points, with $x_1, \ldots, x_N$ on $\partial\Omega$ and a point $x_{N+1} \in \Omega$ and calculate the coefficients α_j by solving the system

$$\tilde{u}(x_i) = \delta_{i,N+1}, \quad i = 1, \ldots, N+1, \tag{10}$$

where $\delta_{i,j}$ is the Kronecker delta.

D. Error Bounds

The algorithm for the eigenmode calculation described in section C provides a solution that satisfies the first condition of problem (1) with a frequency $\tilde{\kappa}$ but not exactly the second condition. Instead of the null boundary condition, the restriction of $\tilde{u}$ to the boundary is a function ϵ which in general is very small. The following result (e.g., [15, 19]) allows to obtain bounds for the error of the eigensolutions which depend on the magnitude of ϵ.

Theorem 3. *Let $\tilde{\kappa}$ and $\tilde{u} \in C^2(\Omega) \cap C(\bar{\Omega})$ be an approximate eigenfrequency and eigenmode which satisfy the following problem:*

$$\begin{cases} \Delta\tilde{u} + \tilde{\kappa}^2\tilde{u} = 0 & \text{in } \Omega \\ \tilde{u} = \epsilon(x) & \text{on } \partial\Omega. \end{cases} \tag{11}$$

Then there exists an eigenfrequency κ_p such that

$$\frac{|\kappa_p - \tilde{\kappa}|}{|\kappa_p|} \leq \theta, \tag{12}$$

where

$$\theta = \frac{\sqrt{|\Omega|}\|\epsilon\|_{L^\infty(\partial\Omega)}}{\|\tilde{u}\|_{L^2(\Omega)}}, \tag{13}$$

and $|\Omega|$ is the volume of the domain Ω. If in addition, $\|\tilde{u}\|_{L_2(\Omega)} = 1$ and u is the normalized orthogonal projection of u onto the eigenspace of κ_p, then

$$\|u - \tilde{u}\|_{L^2(\Omega)} \leq \frac{\theta}{\rho_p}\left(1 + \frac{\theta^2}{\rho_p^2}\right)^{\frac{1}{2}}, \tag{14}$$

where

$$\rho_p := min_{\kappa_n \neq \kappa_p} \frac{\left|\kappa_n^2 - \tilde{\kappa}^2\right|}{\kappa_n^2}. \tag{15}$$

E. Determination of the Eigenfrequencies with Neumann Boundary Condition

In this section, we will describe the application of the MFS for the calculation of the eigenfrequencies for problems with Neumann boundary conditions. We considered approximations of the type

$$u_\omega(x) = \frac{i}{4}\sum_{j=1}^{N} \alpha_j H_0^{(1)}(\omega|x - y_j|)$$

and we know that

$$\frac{\partial J_0(r)}{\partial r} = J_1(r)$$

and

$$\frac{\partial Y_0(r)}{\partial r} = Y_1(r).$$

Then we conclude that

$$\nabla u_\omega(x) = \frac{i}{4}\sum_{j=1}^{N}\alpha_j\omega\frac{x-y_j}{|x-y_j|}H_1^{(1)}(\omega|x-y_j|)$$

where we define

$$H_1^{(1)}(r) = J_1(r) + i\,Y_1(r)$$

and defining

$$\hat{\Phi}(x) = \frac{i}{4}\,H_1^{(1)}(\omega|x|)$$

we have

$$\nabla u_\omega(x) = \sum_{j=1}^{N}\alpha_j\omega\frac{x-y_j}{|x-y_j|}\hat{\Phi}(\omega|x-y_j|).$$

After calculating the unitary vector n that is normal to the boundary at the point $x_i \in \partial\Omega$ we must impose in the system that

$$\partial_n u_\omega(x_i) = \sum_{j=1}^{N}\alpha_j\omega\left\langle n, \frac{x_i-y_j}{|x_i-y_j|}\right\rangle\hat{\Phi}(\omega|x_i-y_j|) = 0.$$

Then the procedure is similar to the Dirichlet case, where instead of the matrix $\mathbf{A}(\omega)$ we have

$$\mathbf{B}(\omega) = \left[\omega\left\langle n, \frac{x_i-y_j}{|x_i-y_j|}\right\rangle\hat{\Phi}(\omega|x_i-y_j|)\right]_{N\times N}. \tag{16}$$

F. Determination of the Eigenmodes with Neumann Boundary Condition

The procedure to calculate approximations to the Neumann eigenmodes is similar to that of the Dirichlet case. Assume that $\tilde{\kappa}$ is an approximation of the eigenfrequency. We consider $N+1$ source points on the artificial boundary and $N+1$ collocation points, N points on $\partial\Omega$ where we impose the Neumann condition $\partial_n u_{\tilde{\kappa}}(x_i) = 0$ and an extra collocation point inside the domain where we impose that $u_{\tilde{\kappa}}(x_{N+1}) = 1$, to exclude the trivial zero solution.

IV. THE METHOD OF PLANE WAVES FORMULATION

In [5] the asymptotic properties of the fundamental solutions were analysed which allowed to suggest another Trefftz type method. Instead of using a linear combination of fundamental solutions it was proposed to use a linear combination of plane waves. The theoretical and numerical results

presented showed that the method produces at least similar (and in some cases better) results to those obtained with the MFS. The completeness of the system of plane waves was already shown in [11]. Next we study the application of that method to the eigenvalue calculation. We consider approximate eigenfunctions

$$u_{\omega}^{PW}(x) = \sum_{j=1}^{N} \alpha_j e^{i\omega x.d_j} \tag{17}$$

with $d_j \in S^{d-1}$, where S^{d-1} denotes the unitary sphere in $\mathbb{R}^d$ and the coefficients α_j are calculated so that the linear combination (17) fits in some sense the boundary conditions of the problem. Then a straighforward procedure to calculate the eigenfrequencies is a collocation scheme. We consider N points x_i uniformly distributed on the boundary of the domain where we impose that the boundary conditions are satisfied. Then we obtain the system of equations

$$\sum_{j=1}^{N} \alpha_j e^{i\omega x_i.d_j} = 0, \quad i = 1, \ldots, N. \tag{18}$$

Therefore a possible way to calculate the eigenfrequencies is to find the values ω for which the $N \times N$ matrix

$$\mathbf{C}(\omega) = [e^{i\omega x_i.d_j}]_{N\times N} \tag{19}$$

has a null determinant or equivalently where the function

$$g(\omega) = \log(|\mathbf{C}(\omega)|)$$

has a singularity. For the particular case of a circular domain we can study the eigenvalues of the matrix associated with the method of plane waves and this allows to show that the roots of the determinant of the matrix converge to the exact eigenfrequencies of the domain.

Proposition 1. *Suppose that Ω is a circular domain, then the roots of the determinant of the plane waves method matrix converge to the eigenfrequencies of Ω.*

Proof. The eigenvalues of a circulant matrix $\mathbf{M} \in \mathbb{C}^{n\times n}$ of the form

$$\begin{bmatrix} a_0 & a_1 & \ldots & a_{n-1} \\ a_{n-1} & a_0 & \ldots & a_{n-2} \\ \ldots & \ldots & \ldots & \ldots \\ a_1 & a_2 & \ldots & a_0 \end{bmatrix}$$

are given (e.g., [20]) by

$$\lambda_k = \sum_{j=0}^{n-1} e^{\frac{2ikj\pi}{n}} a_j, \; k = 0, \ldots, n-1.$$

Applying the method of plane waves for the calculation of the eigenfrequencies of a circular domain, using the determinant root search we start defining some collocation points x_i on the circular domain and directions d_j

$$x_i = R\left(\cos\left(\frac{2\pi i}{n} + \varsigma\right), \sin\left(\frac{2\pi i}{n} + \varsigma\right)\right),$$
$$d_j = \left(\cos\left(\frac{2\pi j}{n} + \varsigma\right), \sin\left(\frac{2\pi j}{n} + \varsigma\right)\right).$$

Then we have

$$x_i.d_j = R\cos\left(\frac{2\pi}{n}(i-j)\right)$$

and the rigidity matrix of the plane waves method is a circulant matrix, where

$$a_j = e^{i\omega R\cos\left(\frac{2\pi}{n}j\right)}, \quad j = 0, 1, \ldots, n-1.$$

Then its eigenvalues are given by

$$\lambda_k = \sum_{j=0}^{n-1} e^{\frac{2i\pi jk}{n}} e^{i\omega R\cos\left(\frac{2\pi}{n}j\right)}, \quad k = 0, 1, \ldots, n-1.$$

This formula can be seen as a quadrature rule converging to the integral

$$\int_0^{2\pi} e^{ikt} e^{i\omega R\cos(t)} dt.$$

and this integral can be written in terms of Bessel functions as

$$\int_0^{2\pi} e^{ikt} e^{i\omega R\cos(t)} dt = \frac{2\pi}{-i^n} J_k(\omega R). \tag{20}$$

The roots of the determinant of the plane waves method are the frequencies such that one of the eigenvalues of the rigidity matrix vanishes and by (20) they converge to the frequencies ω such that $J_k(\omega R) = 0$, for some k. It follows that the roots of the determinant of the matrix of the plane waves method converge to the eigenfrequencies of Ω. ∎

V. SUBSPACE ANGLE TECHNIQUE (SAT)

In section IV, we presented the method of plane waves and the algorithm to calculate the eigenfrequencies searching for the values ω such that the matrix is not invertible. This procedure is very simple and in Proposition 1 we proved that if the domain is circular then the method converges to the exact solutions. However, as we will see below in numerical simulations, due to the ill conditioning, this is no longer possible with more complicated shapes and a more robust technique for eigenfrequency calculation must be considered. One possibility is to use the subspace angle technique (SAT) developed in [4] which makes use of the some classical tools of linear algebra, such as the QR Decomposition and the Singular Value Decomposition.

We will describe an approach for the eigenfrequency calculation based on the subspace angle technique (cf. [4]) explaining the procedure for a general Trefftz type method which includes the MFS and the method of plane waves. We approximate an eigenfunction by a linear combination of some particular solutions ψ_j that satisfy the Helmholtz equation with a frequency ω,

$$u(x) \approx \tilde{u}(x) = \sum_{j=1}^{N} \eta_j \ \psi_j(x). \tag{21}$$

Let x_i^B, $i = 1, 2, \ldots, M_B$ (with $M_B > N$) be points uniformly distributed on the boundary of the domain and x_i^I, $i = 1, 2, \ldots, M_I$ points randomly placed inside the domain Ω. Then define the matrix

$$\mathbf{A}(\omega) = \begin{bmatrix} \mathbf{A}^B(\omega) \\ \mathbf{A}^I(\omega) \end{bmatrix}_{(M_B+M_I)\times N} \tag{22}$$

where

$$\mathbf{A}^B_{i,j}(\omega) = \psi_j\left(x_i^B\right), \quad \mathbf{A}^I_{i,j}(\omega) = \psi_j\left(x_i^I\right)$$

and calculating a QR factorization of $\mathbf{A}(\omega)$ we obtain the matrix

$$\mathbf{Q}(\omega) = \begin{bmatrix} \mathbf{Q}^B(\omega) \\ \mathbf{Q}^I(\omega) \end{bmatrix}_{(M_B+M_I)\times N}.$$

Finally to obtain an approximation for the eigenfrequency we must calculate the smallest singular value of the matrix $\mathbf{Q}^B(\omega)$ which we denote by $\sigma(\omega)$. If we have $\sigma(\omega) \approx 0$, then we have a good approximation to the eigenfrequency (see [4] for details).

ALGORITHM OF THE SUBSPACE ANGLE TECHNIQUE (SAT)

- Choose $N \in \mathbb{N}$, M_B boundary points x_i^B and M_I interior points x_i^I
- Repeat for every ω
  - Build the matrices $\mathbf{A}^B(\omega)$, $\mathbf{A}^I(\omega)$ and $\mathbf{A}(\omega)$ as in (22).
  - Calculate the QR factorization of $\mathbf{A}(\omega)$.
  - Calculate $\sigma(\omega)$, the smallest singular value of the matrix $\mathbf{Q}^B(\omega)$.

This algorithm is independent of the set of particular solutions that we choose. It is therefore applicable, for example, to the fundamental solutions or to the plane waves. We will refer to the application of the subspace angle technique with fundamental solutions and plane waves functions by SAT-MFS and SAT-PWM, respectively.

VI. NUMERICAL RESULTS FOR THE STANDARD MFS

A. Validation of the Algorithms

Distribution of the Collocation and Source Points. We will first illustrate the results for the distribution of collocation points that we proposed. In Figure 4, we plot points on a spheric surface obtained with the standard choice (knots in parallel-meridian coordinates) and with the proposed choice. Our choice produces a more uniform distribution. To make what we want to show clear, we plot only the points on half of the spheric surface. Now we consider two non trivial domains.

We will call by Ω_1 and Ω_2 the nontrivial three-dimensional domains with boundaries defined by

$$\partial\Omega_1 = \left\{(2\cos(t)\cos(s), \sin(t)\cos(s), 2\sin(s) - \sin(s)\cos(2s)) : (t,s) \in [0, 2\pi[\times \left[-\frac{\pi}{2}, \frac{\pi}{2}\right]\right\}$$

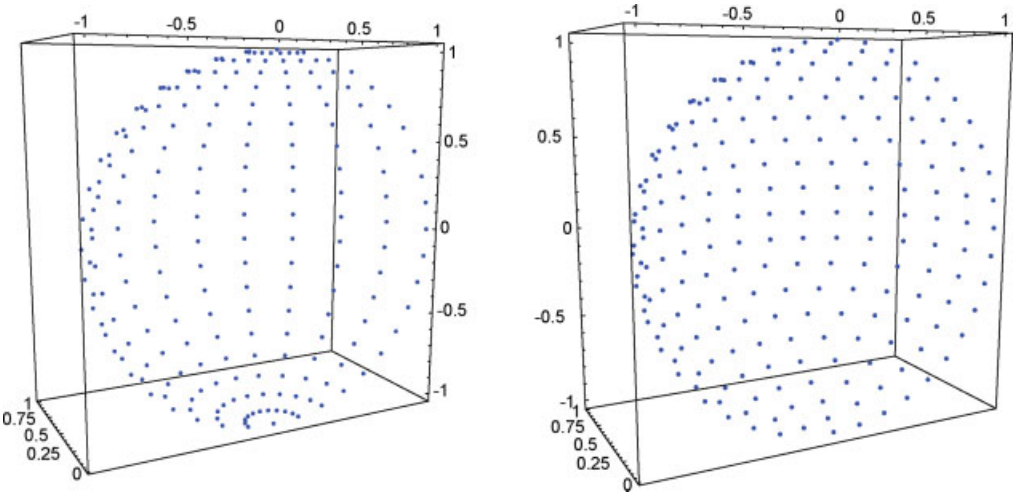

FIG. 4. Plot of the collocation points with the standard and the proposed choice.

and

$$\partial\Omega_2 = \left\{(1.5\cos(t)\cos(s), 1.5\sin(t)\cos(s), \sin(s) - 0.3\cos(2s)) : (t,s) \in [0, 2\pi[\times \left[-\frac{\pi}{2}, \frac{\pi}{2}\right]\right\}.$$

In Figure 5, we plot the collocation points and the source points obtained with the algorithms described in section A and we can observe that the proposed algorithms produces almost uniform distributions.

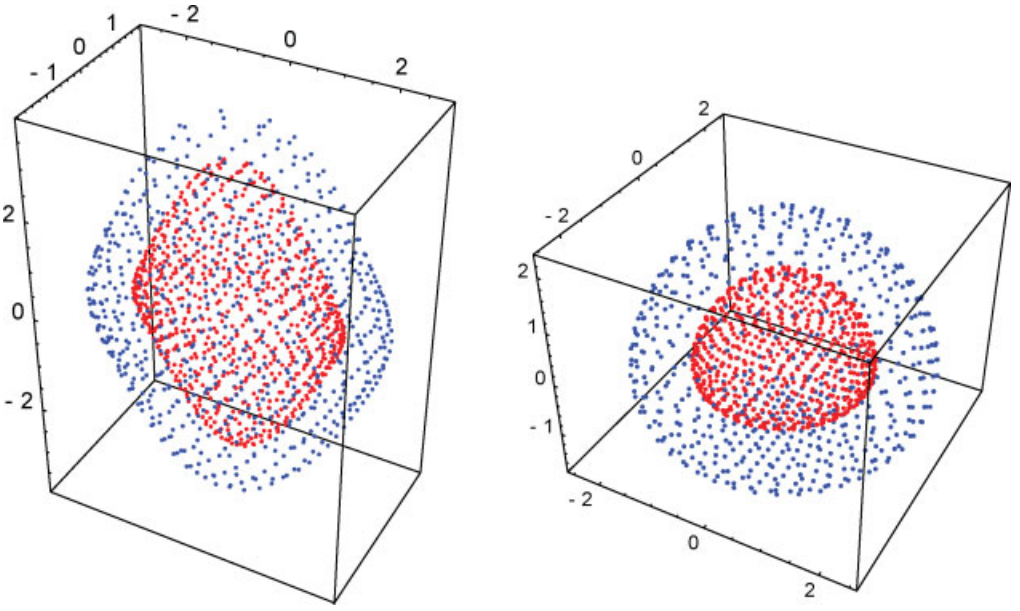

FIG. 5. Collocation and source points for the domains Ω_1 and Ω_2.

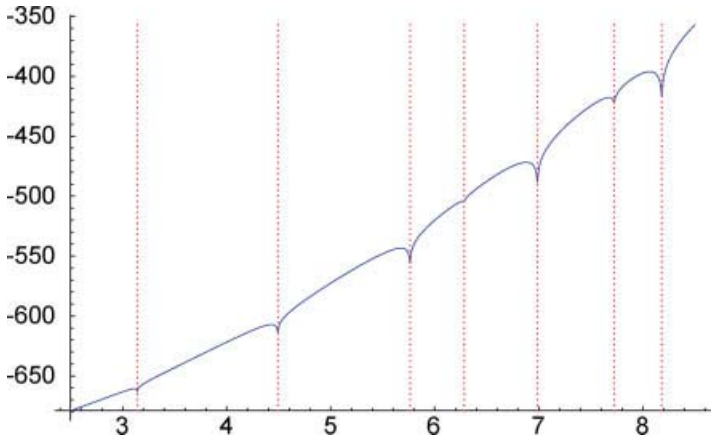

FIG. 6. Plot of $g(\omega)$ for the unit ball with $N = 112$. [Color figure can be viewed in the online issue, which is available at www.interscience.wiley.com.]

Eigenfrequency Calculation—Dirichlet Case. Now we present some numerical results to illustrate the high accuracy that can be achieved with the MFS. In each example, we will refer the value of α that was considered but the method is not much sensitive to other values of α. The eigenfrequencies for the unit ball are well known, and are given by Bessel functions. In Figure 6, we plot $g(\omega)$ for $\omega \in [2.5, 8.5]$ with $N = 112$ and we marked with a dashed red line the exact values. As can be seen, the function has a singularity at each of the eigenfrequencies. To calculate them we apply the golden ratio search. Next we test the results of this method for the three first resonance frequencies of the unit ball considereing $\alpha = 5$. In Table I we show the results obtained with the standard and proposed choices for the collocation points (first plot of Fig. 4). Comparing the results it is evident that the choice of nodes that we proposed produces much better results. For the unit cube we obtain also very accurate results (Table II). The three first resonance frequencies were calculated considering $\alpha = 2$.

Now we will consider a particular class of three-dimensional domains that are defined by $\Omega = \mathcal{O} \times J$, where $\mathcal{O}$ is an arbitrary shaped two-dimensional domain and J is an interval of $\mathbb{R}$.

TABLE I. Absolute errors for the former three modes of the unit ball with the standard choice of points and with the choice proposed (in bold).

	Absolute errors					
N	κ_1		κ_2		κ_3	
112	1.2×10^{-6}	$\mathbf{1.3 \times 10^{-8}}$	2.1×10^{-6}	$\mathbf{9.2 \times 10^{-7}}$	8.9×10^{-4}	$\mathbf{8.6 \times 10^{-6}}$
158	3.7×10^{-8}	$\mathbf{8.6 \times 10^{-12}}$	1.8×10^{-7}	$\mathbf{1.9 \times 10^{-9}}$	2.6×10^{-5}	$\mathbf{6.5 \times 10^{-8}}$
212	3.4×10^{-10}	$\mathbf{2.2 \times 10^{-14}}$	3.7×10^{-9}	$\mathbf{1.6 \times 10^{-13}}$	9.9×10^{-8}	$\mathbf{9.5 \times 10^{-11}}$

TABLE II. Absolute errors for the former three modes of the unit cube.

N	Abs. error (κ_1)	Abs. error (κ_2)	Abs. error (κ_3)
152	2.1×10^{-7}	3.8×10^{-5}	4.9×10^{-5}
218	6.1×10^{-10}	9.3×10^{-7}	1.6×10^{-6}
296	3.1×10^{-10}	7.3×10^{-8}	7.1×10^{-8}
386	9.2×10^{-12}	5.3×10^{-9}	1.9×10^{-10}

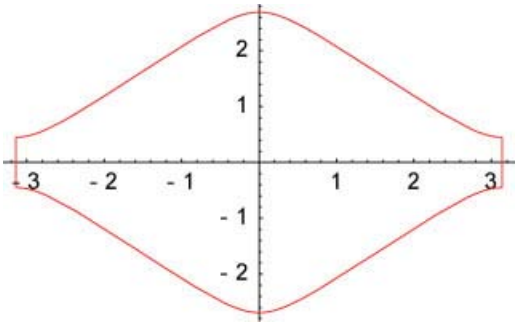

FIG. 7. Plot of the domain D_1. [Color figure can be viewed in the online issue, which is available at www.interscience.wiley.com.]

In this case, if we consider the separation of variables

$$u(x, y, z) = v(x, y)w(z) \tag{23}$$

and denote by $\overset{d}{\Delta}$ the d-dimensional Laplace operator we have

$$\begin{aligned}\overset{3}{\Delta}\, u(x, y, z) &= \frac{\partial^2 v(x, y)}{\partial x^2} w(z) + \frac{\partial^2 v(x, y)}{\partial y^2} w(z) + v(x, y)\frac{\partial^2 w(z)}{\partial z^2} \\ &= w(z)\ \overset{2}{\Delta}\, v(x, y) + v(x, y)\ \overset{1}{\Delta}\, w(z).\end{aligned}$$

Now if we choose v and w such that

$$-\overset{1}{\Delta}\, w(z) = \sigma_1 w(z) \quad -\overset{2}{\Delta}\, v(x, y) = \sigma_2 v(x, y)$$

then

$$-\overset{3}{\Delta}\, u(x, y, z) = \sigma_1 v(x, y)w(z) + \sigma_2 v(x, y)w(z) = (\sigma_1 + \sigma_2)u(x, y, z). \tag{24}$$

This means that if v and w are eigenfunctions of the domains $\mathcal{O}$ and J associated to the eigenvalues σ_2 and σ_1, then the function u in (23) will be an eigenfunction of the domain Ω associated to the eigenvalue $(\sigma_1 + \sigma_2)$. As the one-dimensional eigenvalue problem is easy to solve exactly, this calculations allows to know the exact eigenvalues of some nontrivial three-dimensional domains, for which the exact eigenvalues of the two-dimensional domain $\mathcal{O}$ are known. We start considering the domain $\Omega_3 = D_1 \times [0, \pi]$ where D_1 is the domain plotted in Figure 7. The 15th eigenfrequency for this domain is explicitly known since it was built using the nodal lines of the eigenfunction associated to the second eigenfrequency of the square (see [15]) and we obtain accurate results. The absolute errors shown in Table III were calculated with $\alpha = 3$.

TABLE III. Absolute errors for the 15th eigenfrequency of Ω_3.

N	Abs. error (κ_{15})	N	Abs. error (κ_{15})	N	Abs. error (κ_{15})
226	1.4×10^{-5}	304	5.9×10^{-6}	374	7.2×10^{-8}

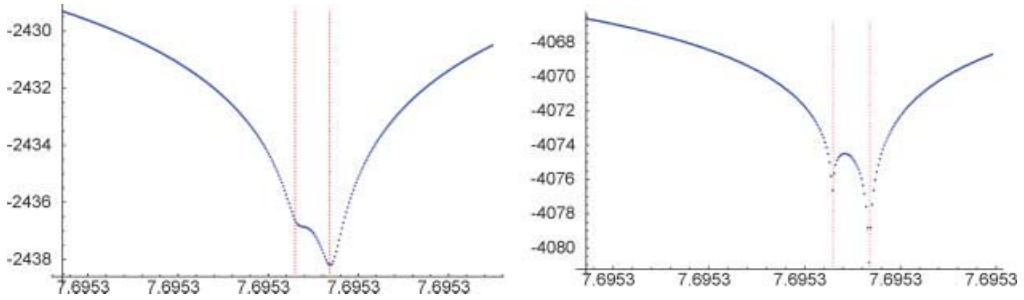

FIG. 8. Plot of $g(\omega)$ for $N = 296$ and $N = 386$.

"Very near" Eigenfrequencies. With the choice of the source points which was described we are able to calculate even eigenfrequencies which are "very near." It is well known that the second eigenvalue of the cube has multiplicity three. Now we consider a rectangular domain with length sides 1, 1 and $1 + 10^{-8}$. For this domain the multiplicity was broken and we have $\kappa_3 - \kappa_2 \approx 3.85 \times 10^{-8}$. In Figure 8 we present the plot of g(ω) for $N = 296$ and $N = 386$ and we obtain the results in Table IV. The method is able to calculate both eigenfrequencies with accuracy.

On the Location of Source Points. To study the effect of the location of the source points we consider the domain $\Omega_4 = D_2 \times [-\frac{\pi}{12}, \frac{\pi}{12}]$ where D_2 is the domain plotted in Figure 9. Following the same procedure as the one described in [15], in this case it is easy to prove that the first eigenfrequency of the domain Ω_4 is $\sqrt{46} \approx 6.7823$. We will consider 324 collocation points on the boundary and three different choices for the source points plotted in Figure 10. In the first two cases we consider the artificial boundary which is (resp.) an "expansion" of the boundary of the domain Ω_4 and a spheric surface. In the last case, we consider the choice of the source points described earlier. In Figure 11, we present the plot of $g(\omega)$ for the points plotted in Figure 10. As can be seen, in the first two cases we have large rounding errors due to the ill conditioning of the matrices that do not allow to locate the singularity. With the choice we proposed the rounding errors are much smaller and the location of the eigenfrequency is evident.

Eigenmode Calculation—Dirichlet Case. Now we will test the results of this method for the calculation of the eigenmodes of the unit cube considering $\alpha = 3$. For simplicity we will consider the eigenmode associated to the first resonance frequency $\kappa = \sqrt{3}\pi$ which has multiplicity one. In Figure 12, we present the plot of the approximation of the eigenmode (calculated using the exact eigenfrequency) for the section $z = 0.25$ and the respective error obtained with $N = 728$. For this section we obtain absolute errors of order 10^{-8}.

Eigenfrequency calculation—Neumann case. Now we will test the results of this method for $\kappa_0 = 0$ and the three first positive resonance frequencies of the unit sphere with Neumann

TABLE IV. Absolute errors for a rectangular domain.

N	Abs. error (κ_2)	Abs. error (κ_3)
386	3.7×10^{-11}	2.4×10^{-11}
488	6.0×10^{-12}	5.1×10^{-12}

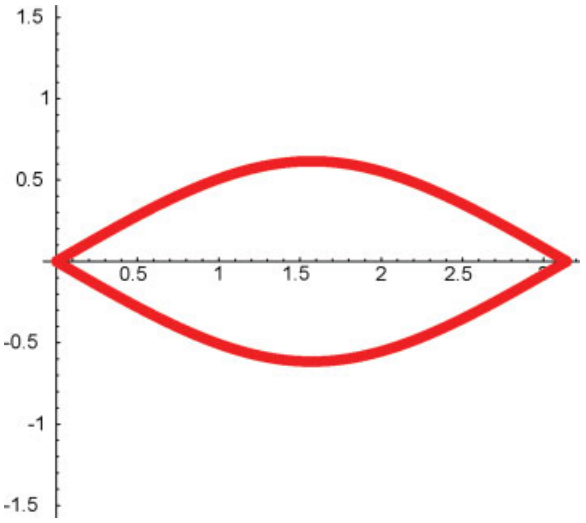

FIG. 9. Plot of the domain D_2. [Color figure can be viewed in the online issue, which is available at www.interscience.wiley.com.]

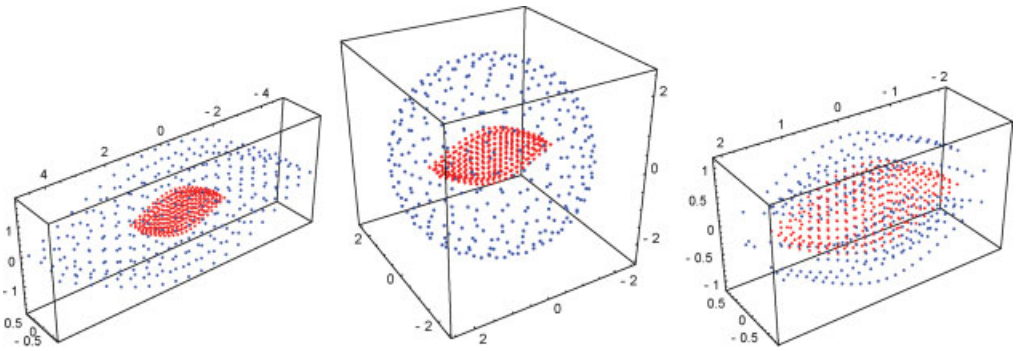

FIG. 10. Collocation points and three choices of the source points for Ω_4.

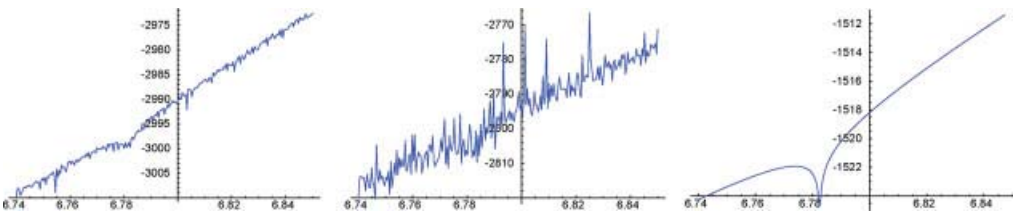

FIG. 11. Plot of $g(\omega)$ for the three different choices of the source points. [Color figure can be viewed in the online issue, which is available at www.interscience.wiley.com.]

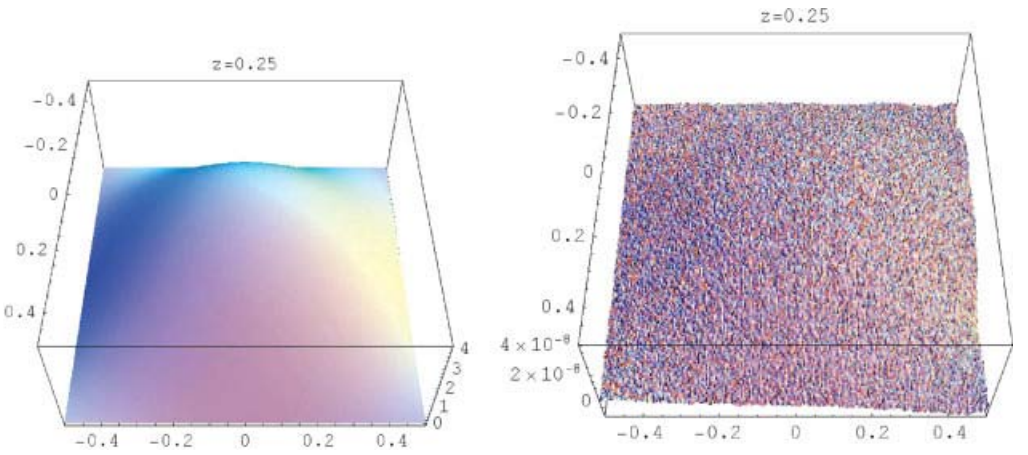

FIG. 12. Plot of the approximation of the eigenmode for $z = 0.25$ and the error. [Color figure can be viewed in the online issue, which is available at www.interscience.wiley.com.]

boundary condition. We obtain the results in Table V (with $\alpha = 5$) and for the unit cube in Table VI (with $\alpha = 2$). In both cases we can see that the method is very accurate.

Eigenmode Calculation—Neumann Case. Now we will apply the method for the eigenmode calculation of the eigenfrequency $\kappa = 2\sqrt{3}\pi$ which has multiplicity one. In Figure 13, we present the plot of the approximation of the eigenmode (calculated with the exact eigenfrequency) for the section $z = 0.25$ and the respective error obtained with $N = 489$. We have absolute error of the eigenmode of order 10^{-9} for this section.

B. Application to NonTrivial Domains

Eigenfrequency/Eigenmode Calculation—Dirichlet Case. To illustrate the performance of the MFS for solving the eigenvalue problem with three-dimensional cavities we will show some numerical results for the domains Ω_1 and Ω_2 which have symmetries. The method behaves well also for domains with smooth boundary with no symmetry. We obtain the results showed in Figure 14 for the eigenmode obtained for the fourth eigenfrequency $\kappa_4 \approx 3.263078$ of domain Ω_1.

TABLE V. Absolute errors for the unit sphere with Neumann boundary conditions.

N	Abs. error (κ_0)	Abs. error (κ_1)	Abs. error (κ_2)	Abs. error (κ_3)
136	3.9×10^{-5}	2.6×10^{-8}	2.1×10^{-7}	1.7×10^{-4}
208	4.2×10^{-6}	6.6×10^{-12}	1.3×10^{-8}	2.4×10^{-6}
312	2.2×10^{-7}	1.7×10^{-12}	7.4×10^{-13}	2.3×10^{-9}

TABLE VI. Absolute errors for the unit cube with Neumann boundary conditions.

N	Abs. error (κ_0)	Abs. error (κ_1)	Abs. error (κ_2)	Abs. error (κ_3)
152	1.7×10^{-4}	1.7×10^{-7}	1.1×10^{-6}	1.2×10^{-7}
218	1.3×10^{-5}	7.6×10^{-9}	9.8×10^{-9}	6.9×10^{-8}
296	1.1×10^{-5}	2.8×10^{-10}	2.0×10^{-10}	8.7×10^{-9}

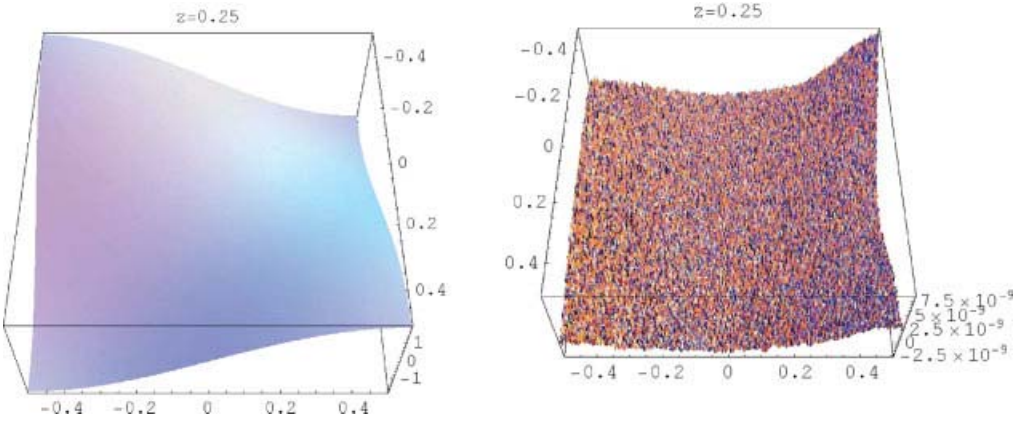

FIG. 13. Plot of the approximation of the eigenmode for $z = 0.25$ and the error. [Color figure can be viewed in the online issue, which is available at www.interscience.wiley.com.]

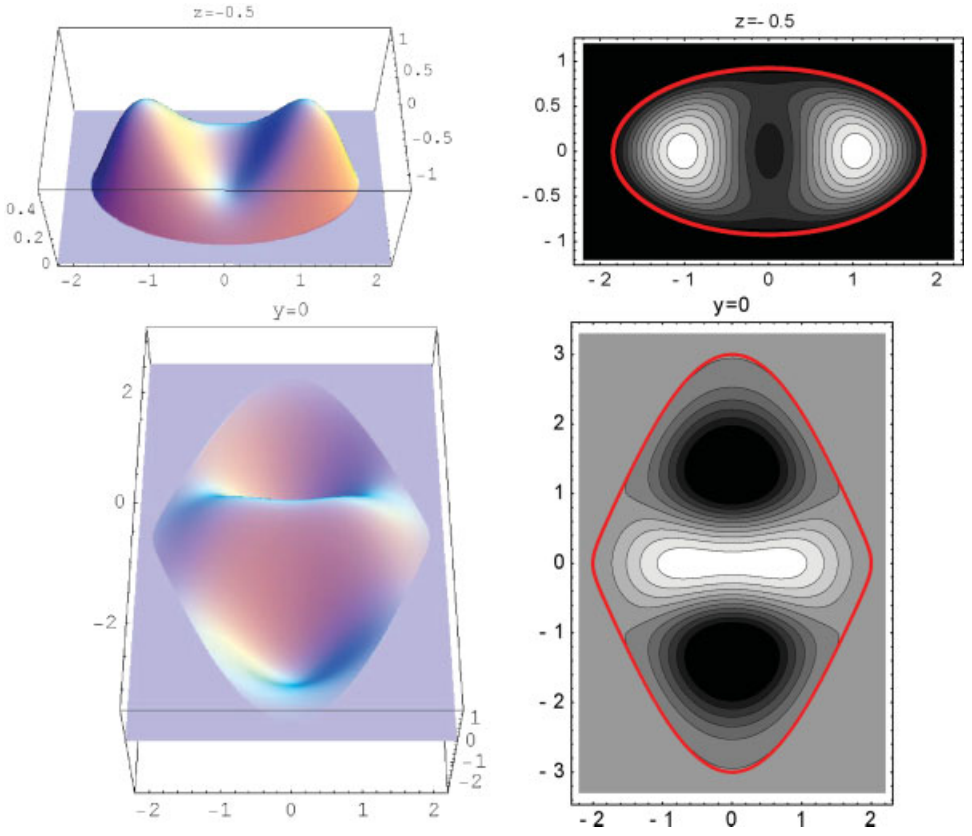

FIG. 14. Plot of sections of the eigenfunction and the respective contourplot for $z = -0.5$ and $y = 0$. [Color figure can be viewed in the online issue, which is available at www.interscience.wiley.com.]

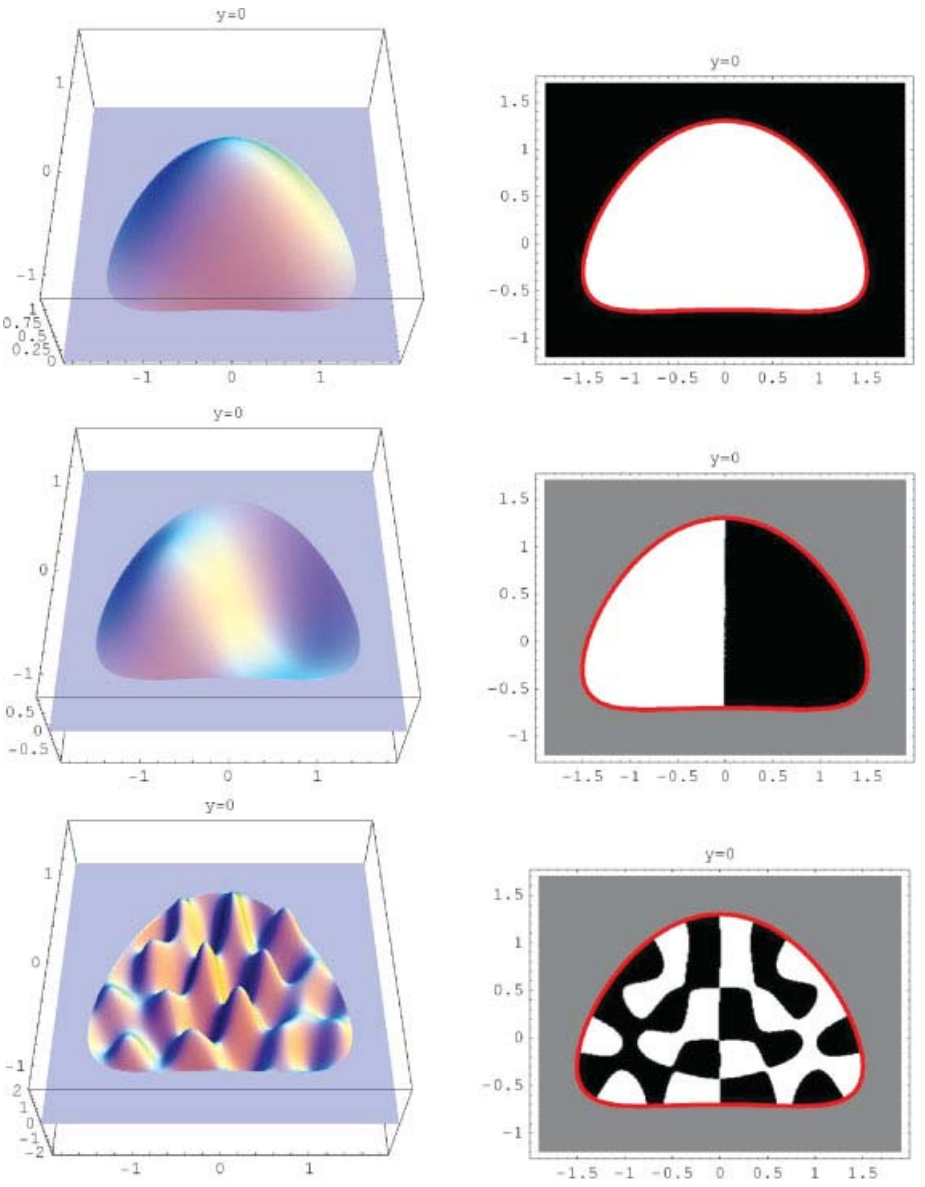

FIG. 15. Plot of sections of the eigenfunctions and nodal domains for $y = 0$. [Color figure can be viewed in the online issue, which is available at www.interscience.wiley.com.]

In Figure 15, we plot sections of the eigenmodes and the respective nodal domains associated with the two first eigenfrequencies and to an high eigenfrequency (we have chosen the 76th) of the domain Ω_2 for the section $y = 0$.

Error Bounds—Dirichlet Case. Using Theorem 3, we calculate bounds for the absolute error of the first two eigenfrequencies and eigenmodes of the domain Ω_2. We obtain numerically that

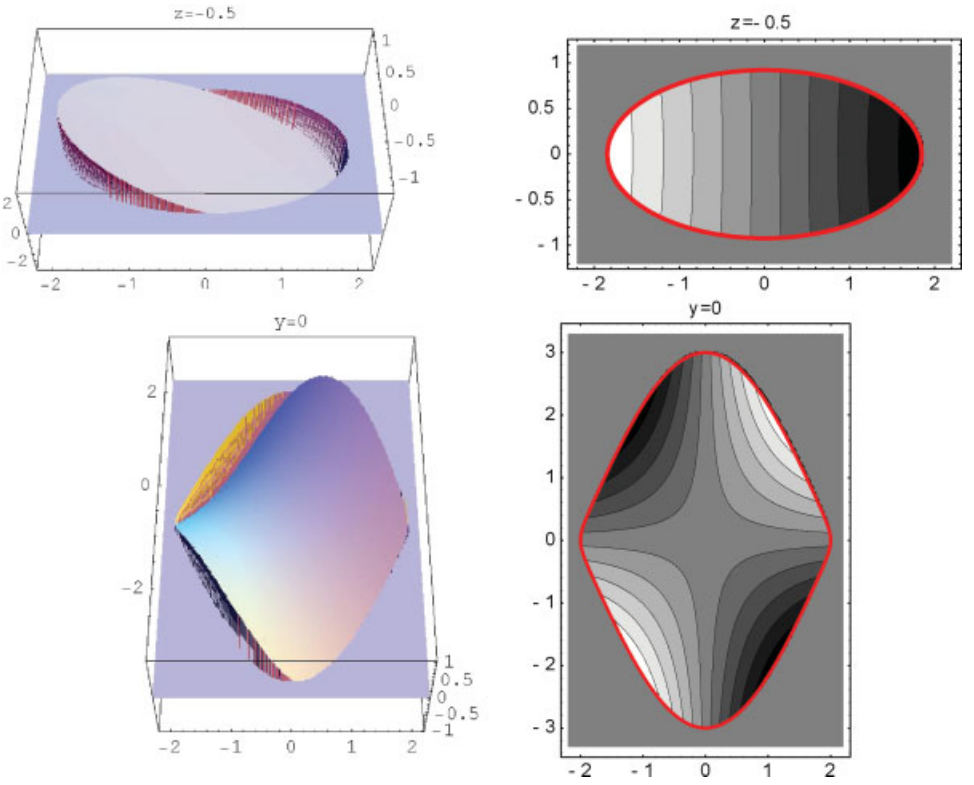

FIG. 16. Plot of sections of the eigenfunction and the respective contourplot for $z = -0.5$ and $y = 0$. [Color figure can be viewed in the online issue, which is available at www.interscience.wiley.com.]

$\theta_1 = 3.41161 \times 10^{-9}$ and $\theta_2 = 5.7429 \times 10^{-9}$. Moreover, $\kappa_3 \approx 3.888566$, so $\rho_1 \approx 0.442046$ and $\rho_2 \approx 0.229901$ and we obtain

$$|\tilde{\kappa}_1 - \kappa_1| \leq 8.7 \times 10^{-9}; \quad |\tilde{\kappa}_2 - \kappa_2| \leq 2.0 \times 10^{-9}$$

and

$$\|u_1 - \tilde{u}_1\|_{L^2(\Omega_2)} \leq 7.72 \times 10^{-9}; \quad \|u_2 - \tilde{u}_2\|_{L^2(\Omega_2)} \leq 2.5 \times 10^{-8}.$$

Eigenfrequency/Eigenmode Calculation—Neumann Case. In Figure 16, we present the results obtained for the eigenmode associated to the fourth Neumann eigenfrequency of Ω_1, $\kappa_4 \approx 1.723454$.

VII. NUMERICAL RESULTS FOR THE MMFS AND THE MMPW

In Figure 17, we plot the results for the convergence of the plane waves method to the first eigenfrequency of the unit ball, for $N = 6, 7, \ldots, 19$. The method shows a very fast convergence and with a small number of points we obtain accuracy close to machine precision.

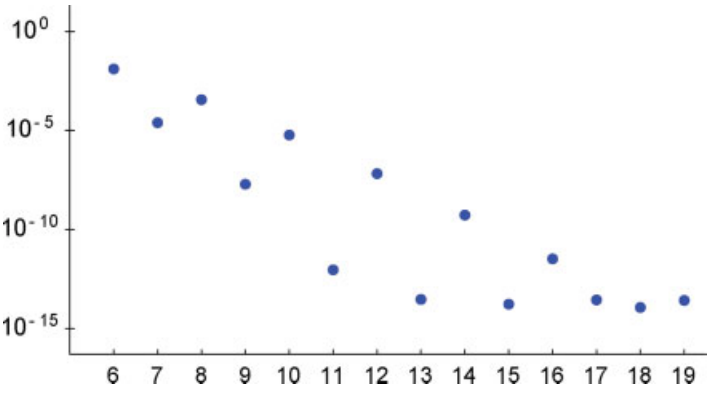

FIG. 17. Convergence to the first eigenfrequency of the unit ball with the plane waves method. [Color figure can be viewed in the online issue, which is available at www.interscience.wiley.com.]

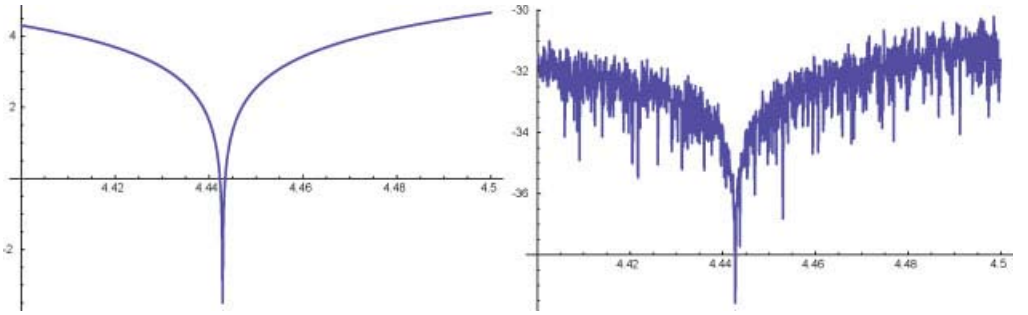

FIG. 18. Plot of $g(\omega)$ for $M = 8$ and $M = 12$. [Color figure can be viewed in the online issue, which is available at www.interscience.wiley.com.]

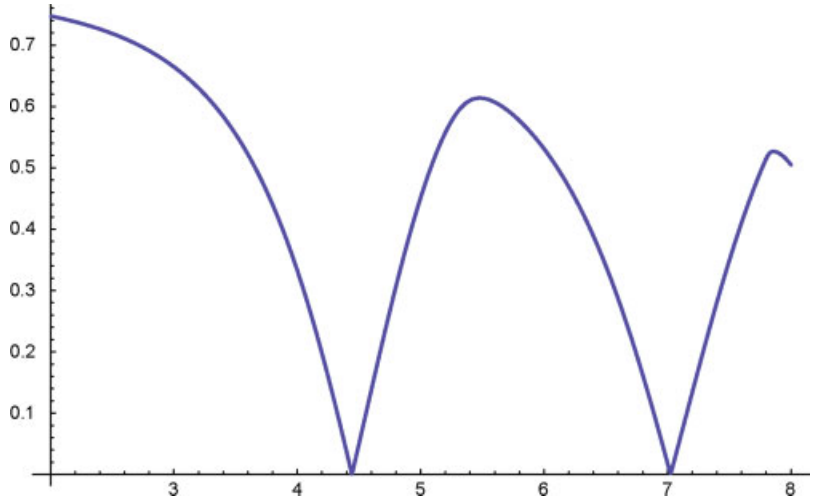

FIG. 19. $\sigma(\omega)$ with the SAT-PWM. [Color figure can be viewed in the online issue, which is available at www.interscience.wiley.com.]

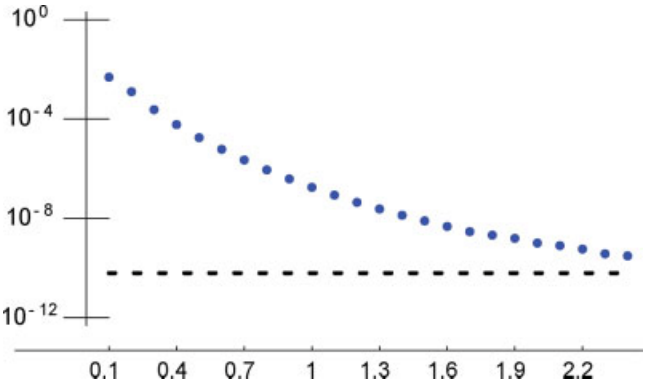

FIG. 20. Absolute error for the SAT-MFS and SAT-PWM (dashed line) for a ball. [Color figure can be viewed in the online issue, which is available at www.interscience.wiley.com.]

However, for more complicated shapes this approach may not be applicable. For example if we consider a unit square with only eigth points we obtain an absolute error near machine precision. Nevertheless, for example with $M = 12$, the rounding errors are very large due to the ill conditioning of the matrix and we can not locate the singularity as shown in the second plot of Figure 18. The same problem happens when we try to apply the method for other shapes.

In Figure 19, we plot $\sigma(\omega)$ for the unit square with the SAT-PWM. We considered $M_B = 50$, $M_I = 20$ and $N = 20$ but the method is not too sensitive to other choices of number of nodes. Using the subspace angle technique, we see that the ill conditioning is circumvented and we can easily calculate the eigenfrequencies. Now we will compare the results obtained with the SAT-MFS and the SAT-PWM. The analytical and numerical results obtained in [5] show that the Method of Plane Waves can be seen as an asymptotic limit of the MFS, when the source points are placed far from the boundary of the domain. In Figure 20, we plot the results for the absolute error obtained (with $M_{\mathrm{B}} = 30$, $M_{\mathrm{I}} = 20$ and $N = 10$) for a unit ball with the SAT-MFS as a function of the distance between the boundary of the domain and the artifial boundary. In Figure 21, we plot similar results for the three-dimensional case with a sphere (with $M_{\mathrm{B}} = 410$, $M_{\mathrm{I}} = 150$ and $N = 150$). In both cases we marked with a dashed line the corresponding value obtained

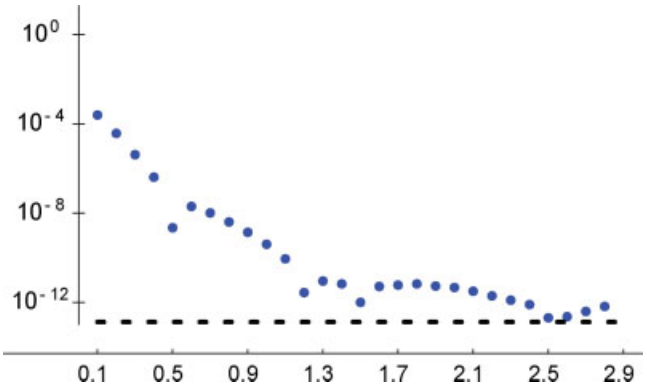

FIG. 21. Absolute error for the SAT-MFS and SAT-PWM (dashed line) for a sphere. [Color figure can be viewed in the online issue, which is available at www.interscience.wiley.com.]

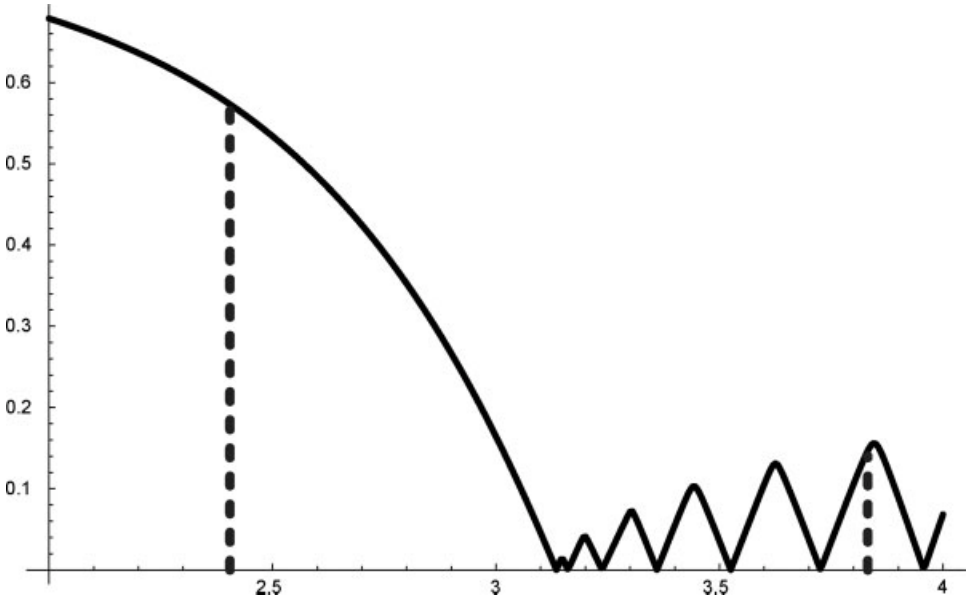

FIG. 22. $\sigma(\omega)$ when apllying the SAT-MFS to an anullar domain.

with the SAT-PWM. We can see that the error decreases when we increase the distance between the boundary of the domain and the artifical boundary. Moreover the result obtained with the SAT-PWM seems to be the limit of the results obtained with the SAT-MFS, as expected. Another advantage of the SAT-MFS when compared with the standard MFS is the absense of spurious eigenvalues when dealing with multiply connected domains. To illustrate this fact, we will apply

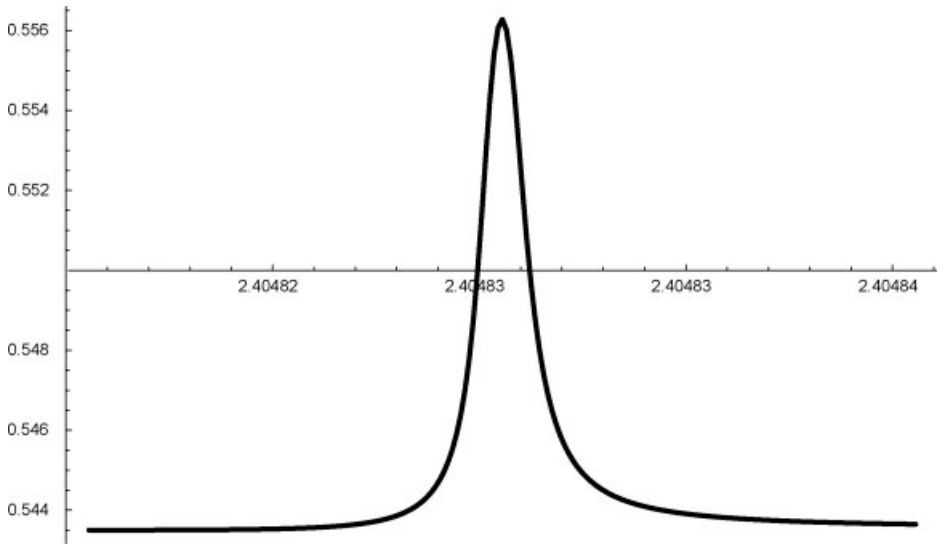

FIG. 23. $\sigma(\omega)$ in a small neighbourhood of the smallest eigenfrequency associated to the inner artificial boundary.

the SAT-MFS to an annular domain with two concentric circular boundaries where the inner and outer radii are 2 and 3 and choose artificial circular boundaries with radii 1 and 7. We place 70 and 100 collocation points on the inner and outer boundaries (resp.); 20 and 30 on the inner and outer artifical boundaries (resp.) and choose randomly 50 points in the domains Ω and we obtain the results of Figure 22. We marked with a dashed line the eigenfrequencies of the Dirichlet eigenvalue problem with the inner artificial boundary which were the spurious eigenfrequencies of the standard MFS as studied in [13] (see also Theorem 2). In that article, the Burton-Miller method and the CHIEF method it were applied to deal with the problem of spurious eigensolutions and both approaches make use of single and double layer potentials. The approach that we described has an advantage when compared with those procedures because only the single layer potential is needed. In Figure 23, we plot $\sigma(\omega)$ in a small neighbourhood of the smallest eigenfrequency associated to the inner artificial boundary. An oscilatory behavior can be observed, but clearly we have $\sigma(\omega) \approx 0$ only for the true eigenfrequencies.

VIII. CONCLUSIONS

We studied the application of the Method of Fundamental Solutions for the calculation of eigensolutions in two and three-dimensional domains. We proposed an algorithm for the choice of collocation and source points which leads to very good results for a quite general class of domains. The study of the application of the Method of the Plane Waves to the eigenvalue problem was also adressed. We considered Dirichlet and Neumann boundary condition and presented some numerical simulations to show the accuracy of the method.

The author thanks Carlos Alves for many fruitful discussions which led to this article. P. R. S. A. was partially supported by FCT, Portugal, through the scholarship SFRH/BPD/47595/2008 and by the project PTDC/MAT/101007/2008.

References

1. G. De Mey, Calculation of the eigenvalues of the Helmholtz equation by an integral equation, Int J Num Methods Eng 10 (1976), 59–66.
2. J. T. Chen, Y. T. Lee, S. R. Yu, and S. C. Shieh, Equivalence between Trefftz method and method of fundamental solution for the annular Green's function using the addition theorem and image concept, Eng Anal Bound Elem 33 (2009), 678–688.
3. J. T. Chen, M. H. Chang, K. H. Chen, and I. L. Chen, Boundary collocation method for acoustic eigenalysis of three-dimensional cavities using radial basis function, Comp Mech 29 (2002), 392–408.
4. T. Betcke and L. N. Trefethen, Reviving the method of particular solutions, SIAM Rev 47 (2005), 469–491.
5. C. J. S. Alves and S. S. Valtchev, Numerical comparison of two meshfree methods for acoustic wave scattering, Eng Anal Bound Elem 29 (2005), 371–382.
6. S. Y. Reutskiy, The method of external sources (MES) for eigenvalue problems with Helmholtz equation, Comput Model Eng Sci 12 (2006), 27–39.
7. V. D. Kupradze and M. A. Aleksidze, The method of functional equations for the approximate solution of certain boundary value problems, USSR Comp Math and Math Phys 4 (1964), 82–126.
8. E. R. Arantes e Oliveira, Plane stress analysis by a general integral method, Proc ASCE Eng Mech Div 94 (1968), 79–101.

9. A. Bogomolny, Fundamental solutions method for elliptic boundary value problems, SIAM J Numer Anal 22 (1985), 644–669.

10. I. Herrera, Trefftz method, Basic principles and applications, C. Brebbia, editor, Topics in boundary element research, Vol. 1, Springer-Verlag, New York, 1984, pp. 225–253.

11. F. J. Sánchez Sesma, I. Herrera, and J. Avilés, A boundary method for elastic wave diffraction. Application to scattering of SH-waves by surface irregularities, Bull Seismol Soc Am 72 (1982), 473–490.

12. A. Karageorghis, The method of fundamental solutions for the calculation of the eigenvalues of the Helmholtz equation, Appl Math Lett 14 (2001), 837–842.

13. J. T. Chen, I. L. Chen, and Y. T. Lee, Eigensolutions of multiply connected membranes using the method of fundamental solutions, Eng Anal Bound Elem 29 (2005), 166–174.

14. C. C. Tsai, D. L. Young, C. W. Chen, and C. M. Fan, The method of fundamental solutions for eigenproblems in domains with and without interior holes, Proc R Soc A 462 (2006), 1443–1466.

15. C. J. S. Alves and P. R. S. Antunes, The method of fundamental solutions applied to the calculation of eigenfrequencies and eigenmodes of 2D simply connected shapes, CMC 2 (2005), 251–266.

16. C. J. S. Alves and C. S. Chen, A new method of fundamental solutions applied to nonhomogeneous elliptic problems, Adv Comp Math 23 (2005), 125–142.

17. P. R. S. Antunes and S. S. Valtchev, A meshfree numerical method for acoustic wave propagation problems in planar domains with corners and cracks, J Comp Appl Math, available at: doi:10.1016/j.cam.2010.01.031.

18. A. Karageorghis, A practical algorithm for determining the optimal pseudo-boundary in the MFS, Adv Appl Math Mech 1 (2009), 510–528.

19. C. B. Moler and L. E. Payne, Bounds for eigenvalues and eigenfunctions of symmetric operators, SIAM J Numer Anal 5 (1968), 64–70.

20. P. J. Davis, Circulant matrices, Wiley-Interscience, New York, 1979.